Thermal and Mechanical Behavior of Copper Molds during Thin-Slab Casting (II): Mold Crack Formation

JOONG KIL PARK, BRIAN G. THOMAS, INDIRA V. SAMARASEKERA, and U. SOK YOON

The formation of cracks in a funnel mold of thin-slab casting is investigated using metallographic studies and mathematical models. In Part II of this two-part article on thin-slab casting molds, short longitudinal cracks near the meniscus region of a thin-slab funnel mold are studied metallurgically. X-ray analyses revealed the formation of Cu-Zn brass on the copper matrix at high temperature where the crack initiated. Heat-transfer and thermal-elastic-viscoplastic stress models described in Part I are applied to investigate the temperature and stress fields associated with the cracks. Large cyclic inelastic strains were found in the funnel transition region just below the meniscus due to the slightly higher temperature at that location. The cracks then appear to have propagated by thermal fatigue caused by major level fluctuations at transitions. The stress and strain predictions suggest cycles to failure for molds for various hot-face temperatures.

I. BACKGROUND

THE thin-slab mold for continuous casting of steel is prone to surface crack formation, particularly in funnel-shaped molds. This is likely associated with the higher casting speeds needed for this increasingly popular process to be efficient. Higher casting speeds generate higher heat flux, which causes greater temperatures and stresses in the mold. Cracks pose a serious quality problem, in addition to the obvious loss of mold life. This is because meniscus cracks may locally retard cooling of the steel shell beneath them and lead to longitudinal crack formation and other defects in the steel product. Despite its importance, the thermomechanical behavior of the mold and mold crack formation has received little attention and is not fully understood.

The present work was undertaken to investigate crack formation in thin-slab molds. In Part I of this two-part article, the thermal and mechanical behavior of both parallel and funnel thin-slab molds were investigated quantitatively based on plant measurements and three-dimensional (3-D) elasto-plastic-creep finite-element models. Part II of this work applies these models together with a metallurgical analysis of the cracks in order to gain new insight into the mechanism of mold crack formation.

II. PREVIOUS WORK

A few previous studies have investigated mold defects, including mathematical models and microstructural analysis to study mold crack occurrence.[1–5] Grill *et al.*[1] investigated mold wear and reported that physical abrasion of the mold is related to the normal force, which acts against the copper faces. Wear occurs in regions of the mold where the air gap is fully closed. Won *et al.*,[2] using a two-dimensional (2-D) coupled thermo-elasto-plastic finite-element model of conventional slab casting, reported that wear increases with increasing narrow-face taper. The width of the worn region was predicted to decrease with increasing carbon concentration in the steel.[2]

H. Gravemann *et al.*[3] analyzed surface cracks in a copper-billet casting mold. These cracks are characterized by transgranular crack propagation. Corrosion fatigue was determined to be the cause and zinc and sulfur to be the corroding media. They also found that in a chrome-plated mold, the corrosion of the copper starts under microcracks in the chrome layer forming the brittle intermetallic phases of beta and gamma brass and/or copper sulfide. Fracture of these brittle compounds leaves notches, which act as stress raisers. With alternating thermal stresses from thermal cycling, these notches ultimately develop into cracks that are 10-mm deep.

Hawbolt *et al.*[4] also studied mold cracks in billet molds and found intergranular cracks combined with the presence of a Zn-rich and Pb-rich phase, suggesting that the copper plate may have undergone a liquid-phase embrittlement when subjected to a tensile stress at very high temperature.

O'Connor and Dantzig[5] computed cyclic inelastic strains in a funnel-shaped thin-slab casting which reached 1.75 pct in a region below the meniscus along the funnel edge. These large strains resulted from the combination of locally high temperatures coupled with the geometric constraint of the mold. Longitudinal fatigue cracks on the hot face were attributed to overconstraint of the copper plates. They suggested cracks could be avoided by loosening the tension bolts connecting the mold with the water jacket in order to allow the mold to move freely parallel to the broad face. They also predicted the cycles to failure for molds. Important, but complicated phenomena, such as the effect of the water-box partial constraint and 3-D behavior, were not considered.

Most previous research has focused on conventional casting, which has relatively lower mold temperatures due to the lower heat flux at the lower casting speeds (1 to 2.5 m/min) relative to thin-slab casting (3.5 to 5 m/min). Despite

JOONG KIL PARK, Graduate Student, and INDIRA V. SAMARASEKERA, Professor, are with the Department of Metals and Metallurgical Engineering, University of British Columbia, Vancouver, BC, Canada V6T 1Z4. Contact e-mail: vpr@exchange.ubc.ca BRIAN G. THOMAS, Professor, is with the Department of Mechanical and Industrial Engineering, University of Illinois at Urbana-Champaign, Urbana, IL 61801. U.-SOK YOON, Senior Researcher, is with the Iron & Steelmaking Research Group, Technical Research Laboratory, POSCO, Pohang, Kyungbuk, Korea.

Manuscript submitted May 29, 2001.

the high level of understanding that has been achieved, several questions of practical importance to mold crack formation remain to be answered. Why does a funnel mold have more cracks than a parallel mold? Why do cracks not always form at the transition area of the funnel mold, where O'Connor found the highest stress? What is the effect of the mold alloy? How many cycles to failure can an ordinary mold withstand with no constraint problems? What is the relative importance of thermal cycling due to metal-level fluctuation compared with major level changes when emptying and refilling the mold? This work aims to investigate some of these issues.

III. MORPHOLOGY OF MOLD CRACKS

Thin-slab casting molds still suffer from mold cracks, despite having implemented the suggestion of minimizing constraint by employing oversized bolt holes (Part I). The first step of this study was to perform a metallurgical analysis of typical mold cracks obtained from an operating thin-slab casting funnel mold after 345 heats of casting.

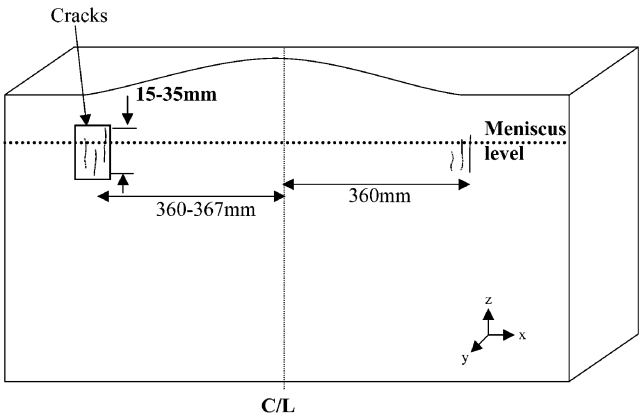

Fig. 1—Schematic diagram of the funnel mold showing the location of mold cracks.

Photographs and micrographs of the mold cracks of interest in this study are presented in Figures 2 through 5. Sometimes, cracks were observed after only 2 or 3 casting sequences, but at other times, molds were in service with no cracks for up to 70 sequences. Figure 1 shows a schematic funnel mold illustrating the location of the mold cracks. Most of the cracks formed just below the meniscus and were located about 360 mm from the center of mold at the transition region of the funnel shape in the same location as observed by O'Connor and Dantzig.[5] A closer examination of the mold surface around the crack reveals two distinct regions, which are identified in Figure 2. The top and bottom part of the specimen are dark gray (Figure 2(a)), which corresponds to the Cr-coating layer. The region around the crack, which is found near the meniscus, is yellow (Figure 2(b)). The composition of this thin layer was identified as a brass, using the energy-dispersive spectrum (EDS) on the scanning electron microscope (SEM) (Figure 6).

Figure 3 shows a transverse section through the mold crack, which penetrates to a depth of about 2.8 mm below the mold surface. The crack seems to be intergranular just below the mold surface, but most of its interior length has the characteristic features of transgranular fracture. This is verified from an SEM fracture analysis in Figure 4, which shows the intergranular fracture surface found just beneath the mold surface. Figure 4 also shows a wedge crack at the triple point of grains, which is characteristic of creep fracture at high temperature. An examination of the fracture surface at the crack root in Figure 5 reveals another fracture morphology that is believed to be fatigue striations. These analyses suggest that the crack is initiated at the surface at high temperature and is then propagated deeper by alternating thermal stress at lower temperature. This transgranular fatigue-crack propagation at lower temperatures is consistent with previous research.[3,6–8] The high-temperature intergranular fracture is consistent with observations of Ashida and Takao[7] for all dispersive Cu alloys including Cu-Cr-Zr. However, it contrasts with H. Gravemann *et al.*[3] and Collins and Taplin[6] reports for the Cu-Cr-Zr alloy, where zirconium was found to segregate to grain boundaries. This

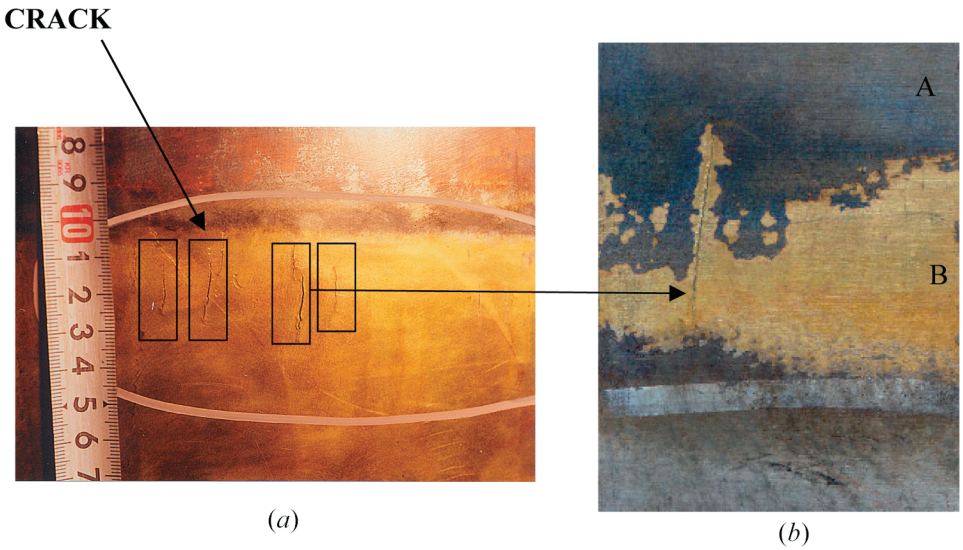

Fig. 2—(*a*) Photograph of the mold crack and (*b*) magnified view.

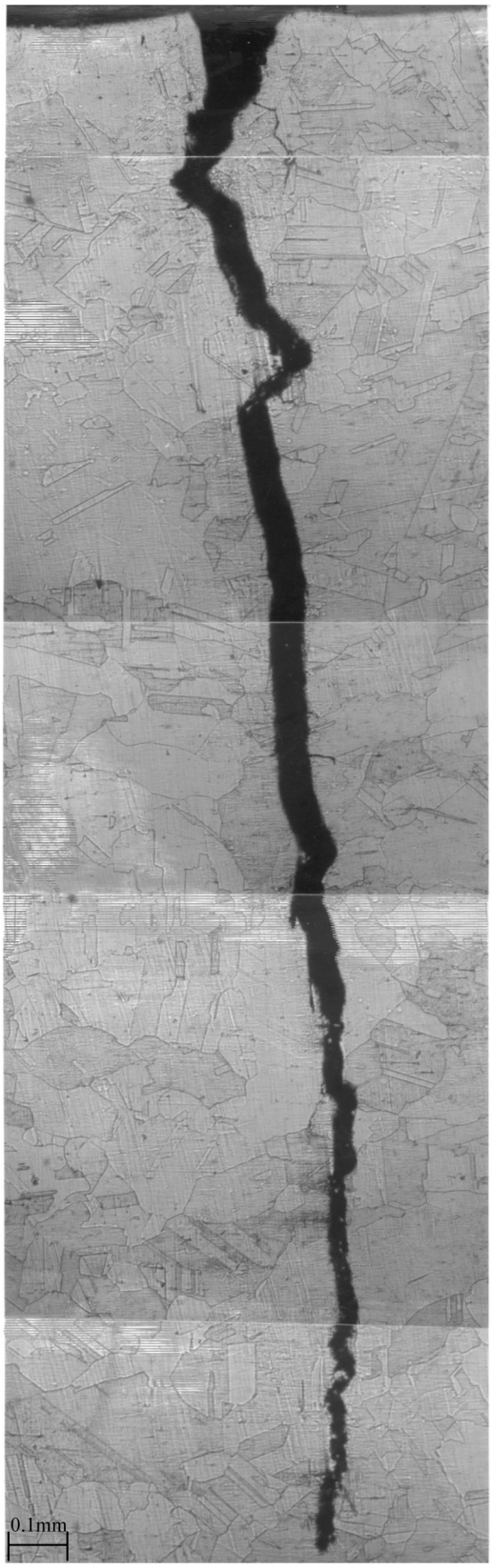

Fig. 3—Optical micrograph of the cross section of the mold crack.

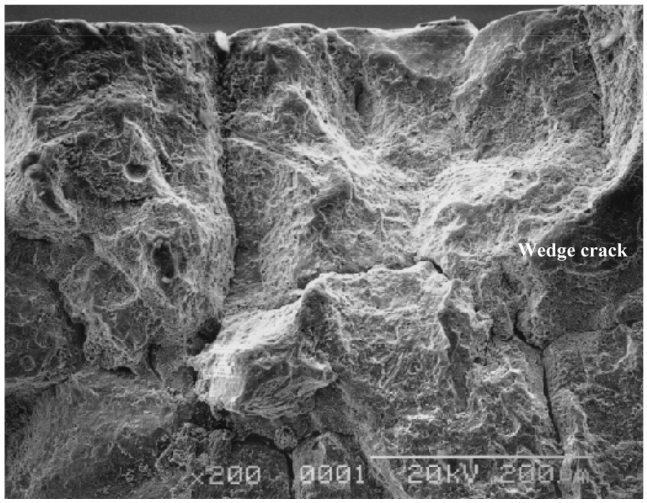

Fig. 4—Fractographs of the mold cracks just below the mold surface showing the intergranular fracture and wedge cracks at the triple point of grain boundary.

Table I. Simulation Conditions for 2-D Slice Modeling

Mold Type	Parallel Mold	Funnel Mold
Copper plate thickness (mm)	60	57 to 80
Mold width (mm)	1660	
Copper alloy	0.5 wt pct Cr − 0.1 wt pct Zr	
Water slot-hot face distance (mm)	25	25 to 27
Bolt length (mm)	445	
Bolt diameter	16	
Bolt hole diameter in water box (mm)	24	
Water slot heat transfer coefficient (W/m^2K)	38.45	
Cooling water temperature (°C)	38	

Table II. The Maximum Displacement (in Millimeters) at the Tension Bolt of Outer-Backing Plate after 50 Sequences of Casting (3-D Quarter Model)

Bolt Position (from Center of Mold)	Width Displacement (after Cooling)		Thickness Displacement (during Operation)	
	Parallel	Funnel	Parallel	Funnel
0	−0.002	−0.003	0.136	0.209
188	0.005	0.005	0.169	0.243
376	0.008	0.009	0.225	0.306
564	0.016	0.017	0.285	0.380
752	0.019	0.021	0.348	0.461

was proposed to be beneficial by forming large harmless precipitates, which decrease stress concentration, avoid grain boundary sliding, prevent void initiation around precipitates, and avoid intergranular fracture.[3,6] Solid-solution-strengthened materials, such as Cu-Ag alloys, are known to have higher fatigue resistance, particularly against intergranular fracture.[7]

Another striking feature of the crack occurrence is that near the top surface of the mold, the Cr-plated layer is absent from around the crack, as shown in Figure 6. Instead of the Cr layer, a brass layer was formed just beneath the hot face of the mold, in which the Zn concentration reached up to

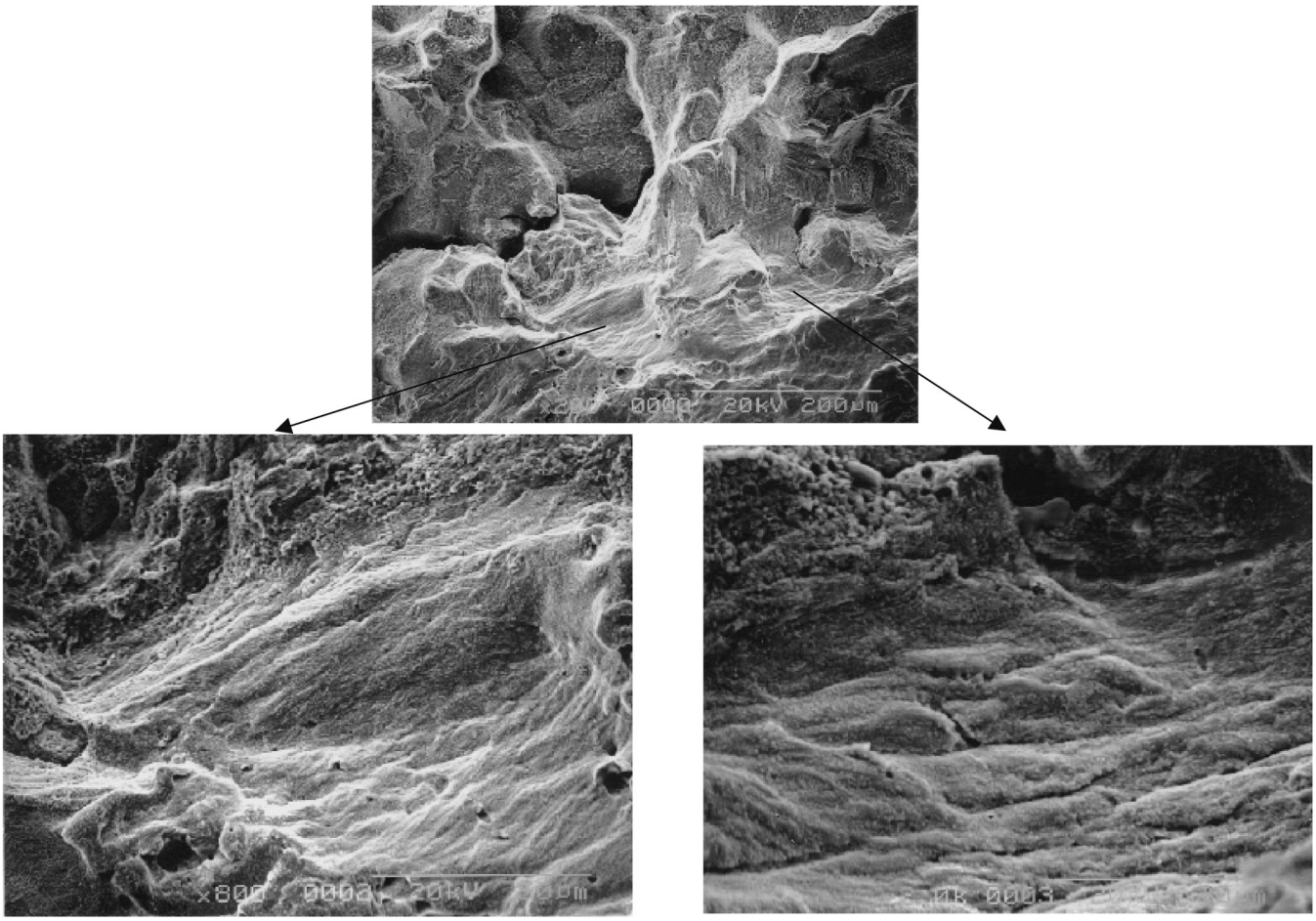

Fig. 5—Fractographs of the mold crack near the crack root showing the striation structure.

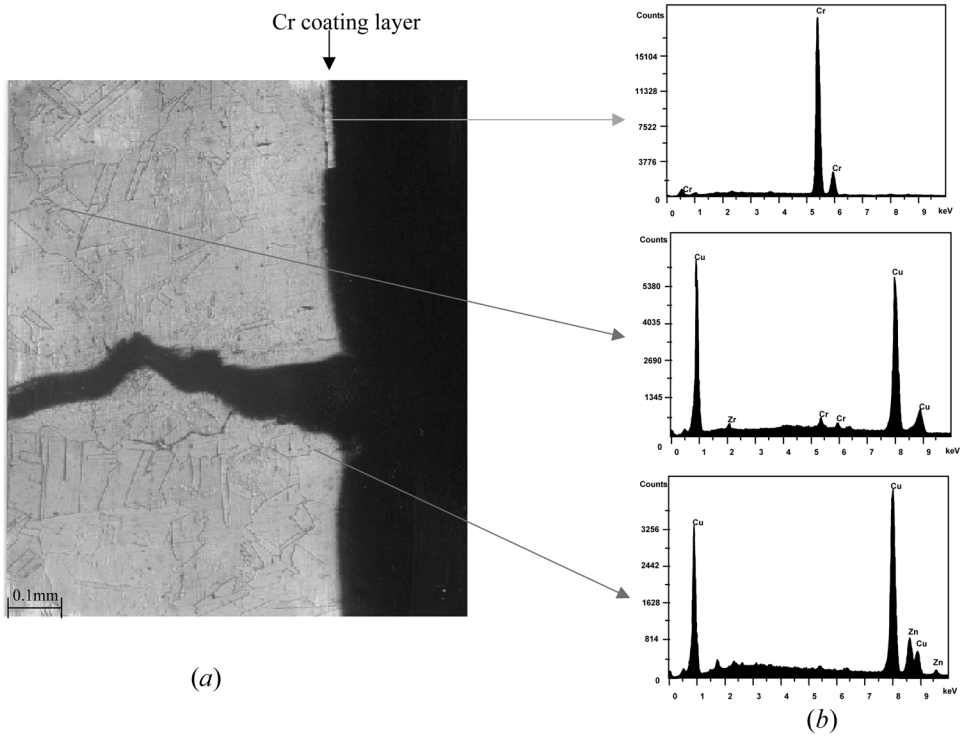

Fig. 6—Optical micrograph of the (*a*) mold crack around the top of crack and (*b*) x-ray spectrum.

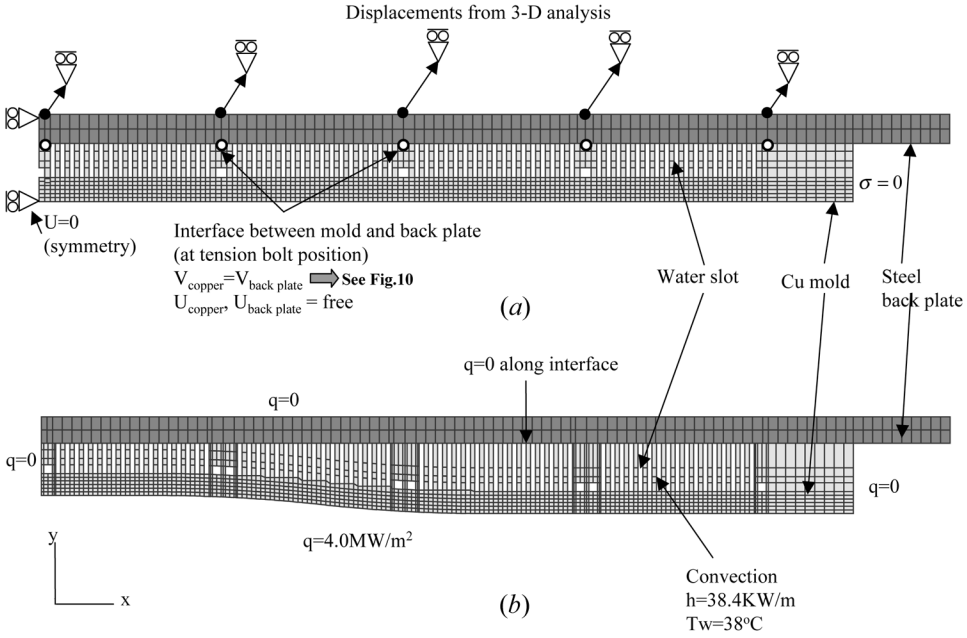

Fig. 7—Finite-element mesh of the 2-D horizontal domain for parallel and funnel molds and its thermal and mechanical boundary conditions: (*a*) parallel mold and stress BC and (*b*) funnel mold and heat BC.

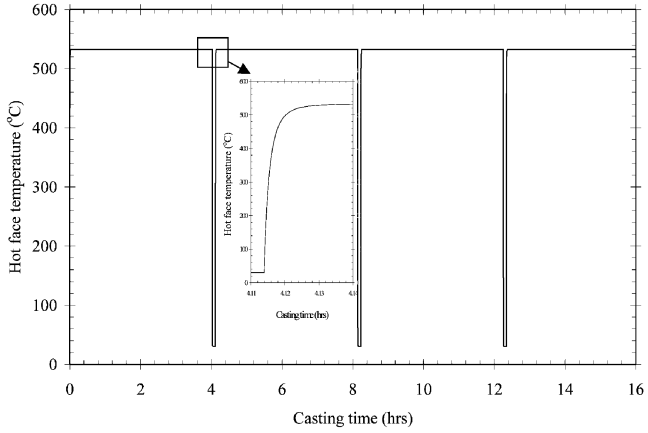

Fig. 8—Thermal pattern of the hot face imposed on the 3-D stress analysis.

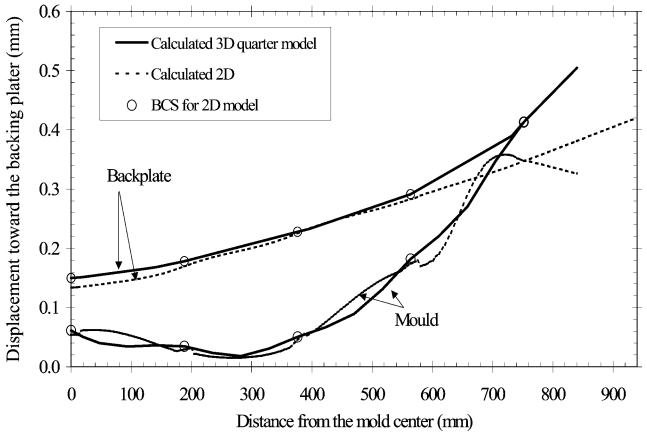

Fig. 10—Vertical displacement across the mold width at the interface of the mold and back plate during the operation for the parallel.

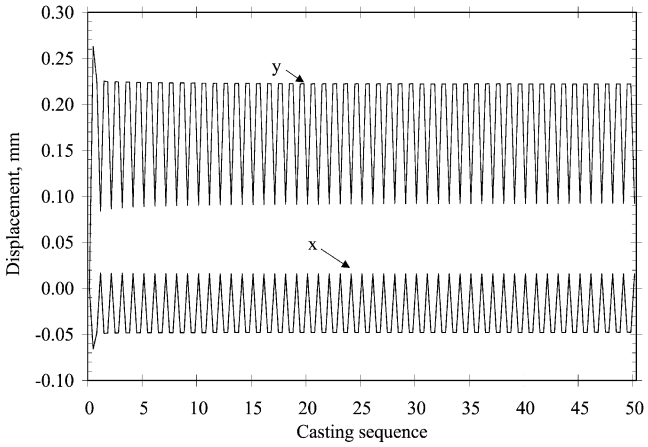

Fig. 9—The change of displacement at a location of 376 mm from the center of the backing plate with casting sequence at the meniscus of the parallel mold.

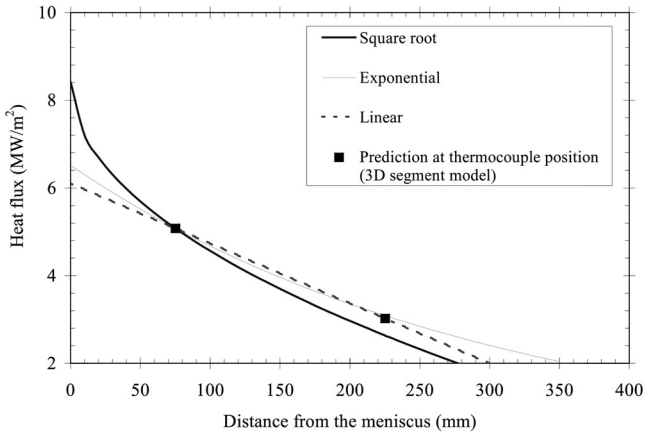

Fig. 11—Comparison of the heat flux profiles at the meniscus region.

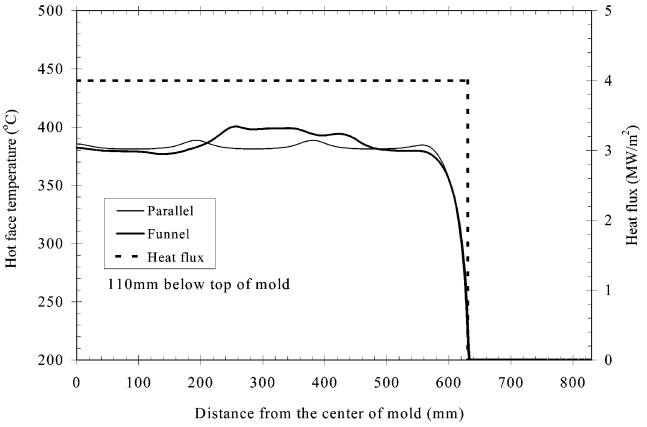

Fig. 12—Comparison of the hot-face temperature distribution of the hot face across the wide face with different mold shapes (2-D quarter model).

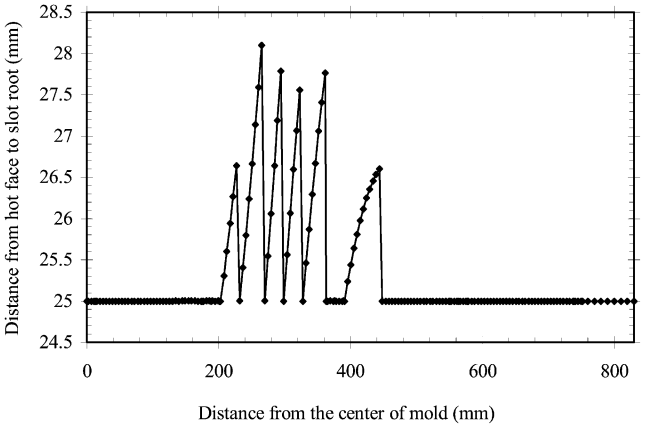

Fig. 13—Slot depth profile across the mold width at the meniscus for the funnel mold.

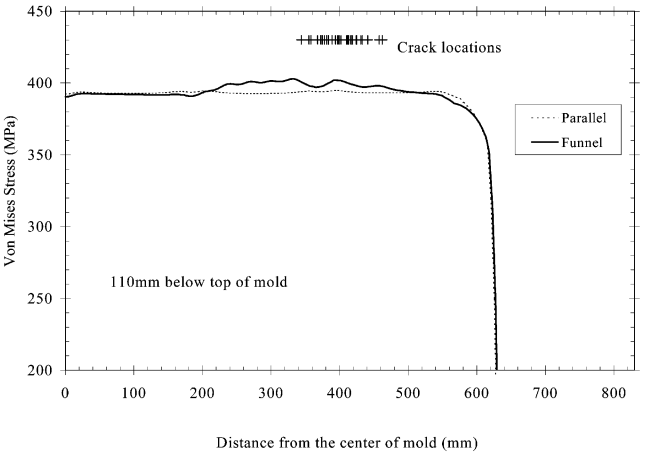

Fig. 14—Comparison of Von Mises stress across the hot face with different mold shapes.

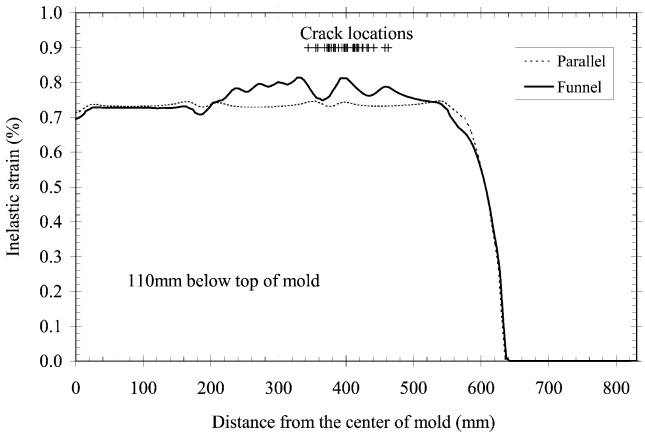

Fig. 15—Comparison of the inelastic strain distribution across the hot face with different mold shapes.

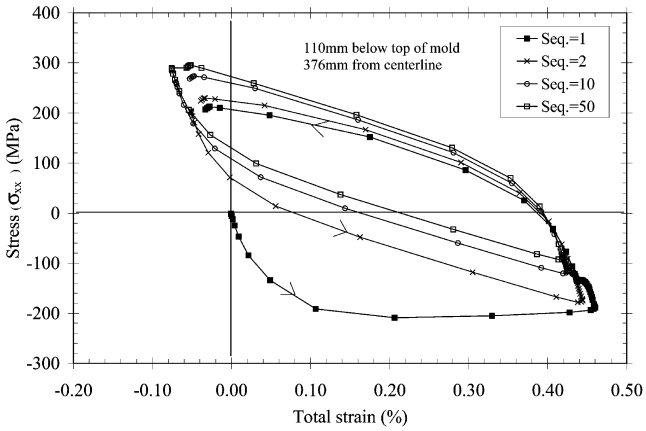

Fig. 16—Stress-strain hysteresis loop on the hot face of the parallel mold.

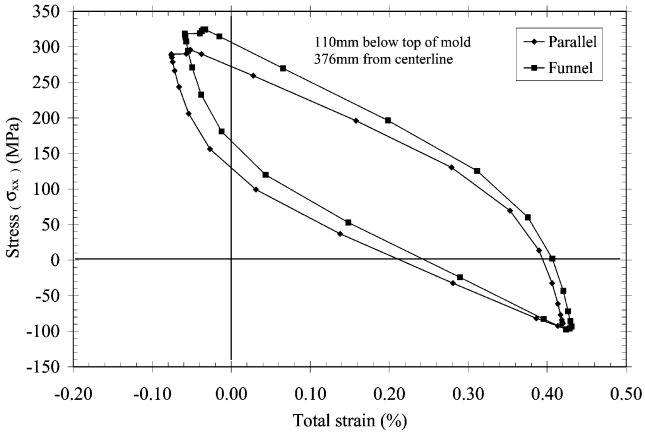

Fig. 17—Comparison of the stress-strain hysteresis loop after 50 sequences.

16 pct, as shown from EDS analysis. The only possible zinc source appears to be the molten metal, which varied from 10 to 20 ppm Zn or higher (up to 60 ppm), depending on the scrap and dust composition in the electric furnace. Zinc absorption into the hottest portion of the mold surface was also reported by O'Connor and Dantzig[5] but only where its temperature exceeds 425 °C. These results suggest that the hottest portion of the hot face of the copper lost its protective Cr layer, exceeded 425 °C, was severely attacked by Zn in the molten metal, and formed brass. Once zinc attacks the copper plate, it preferentially diffuses along the grain boundaries rather than the matrix. This makes the grain boundaries more susceptible to cracks. Once a short crack

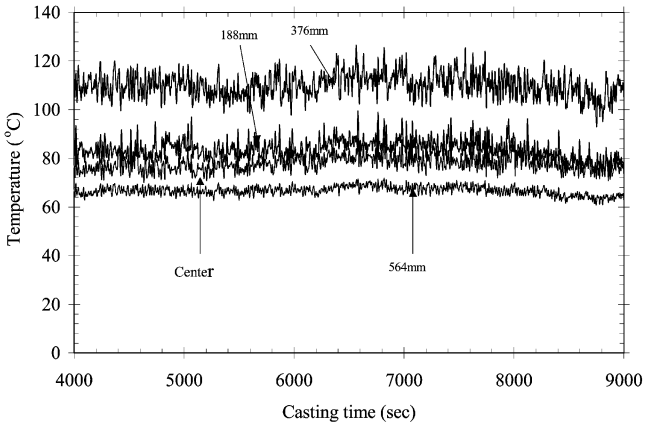

Fig. 18—Temperature response measured in the funnel mold at the meniscus during steady state (100 mm below the mold top).

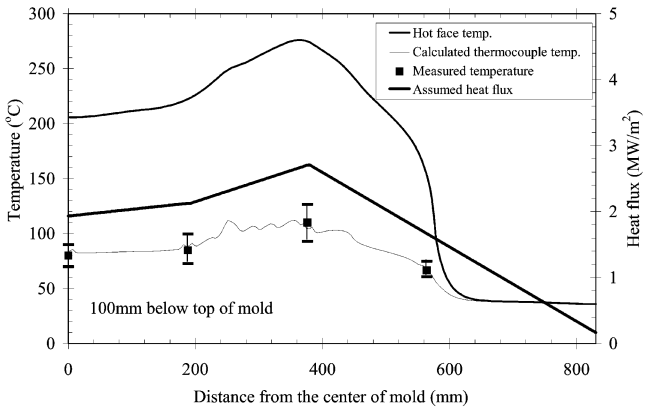

Fig. 19—Comparison of calculated and measured temperatures and corresponding hot face temperature and heat flux profiles across the wide face at the meniscus of funnel mold (2-D quarter model).

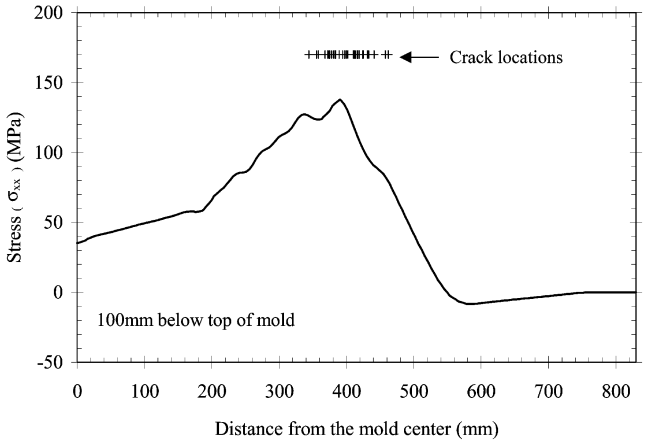

Fig. 20—Stress (σ_{xx}) profile across the wide face of the funnel mold.

is initiated, its tip acts as a stress raiser for crack propagation *via* transgranular thermal fatigue.

IV. THERMAL STRESS MODEL DESCRIPTION

Several models are used to investigate the effect of mold geometry and temperature profiles on the thermal mechanical behavior, its associated crack occurrence, and failure

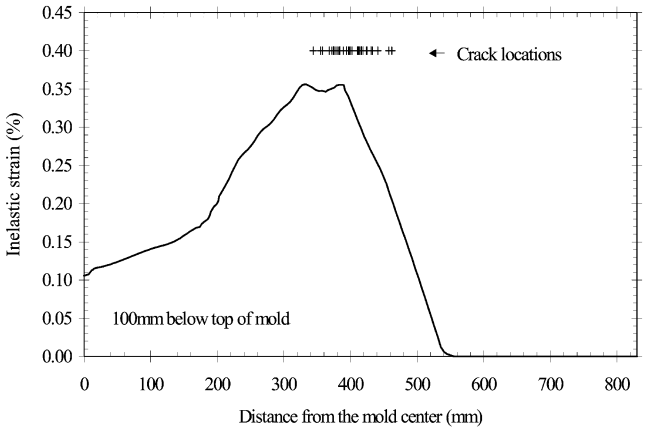

Fig. 21—Inelastic strain profile across the wide face of the funnel mold.

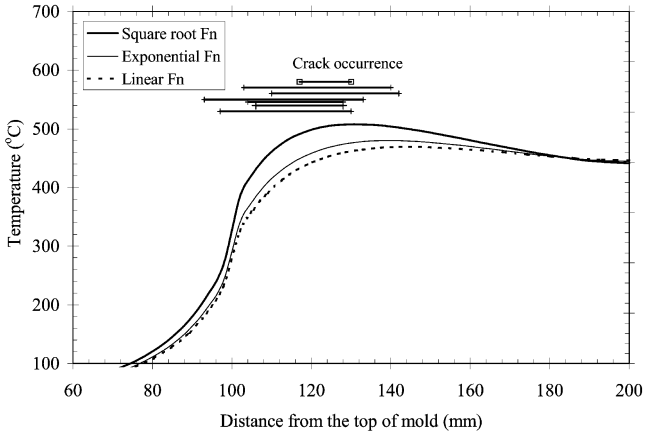

Fig. 22—Effect of the heat-flux profile uncertainty on the hot face temperature predictions (steady 3-D segment model).

criteria for copper thin-slab casting molds. The 2-D finite-element models are applied to calculate temperature and the corresponding stress and strain fields in the parallel and funnel mold using the commercial stress-analysis package, ABAQUS 5.8.[9] Simulation conditions are given in Table 1 and in Part I of this two-part article. Horizontal sections of one-quarter of the mold (2-D quarter model), including part of the water jacket, were taken at the height corresponding to the highest mold temperature, as shown in Figure 7. These slice sections were assumed to deform in plane strain. This section is reasonable because the surface cracks were always longitudinal along the mold length.

To obtain accurate predictions from a 2-D model of 3-D phenomena, special boundary conditions were developed in order to match the 3-D model predictions. First, heat-flux boundary conditions at the hot face of the 2-D quarter model were chosen to be lower than physically measured (Part I) in order to match the temperature predictions of the full 3-D segment model. To obtain boundary conditions for the stress model, the 3-D quarter model was first run, based on the thermal load described in Part I, to reproduce 50 thermal cycles experienced in the real mold shown in Figure 8. Symmetry planes at the wide-face centers are mechanically constrained to prevent normal displacements. To realize the pretension force in the 2-D quarter model, the x and y displacements of the backing plate at each tension-bolt position

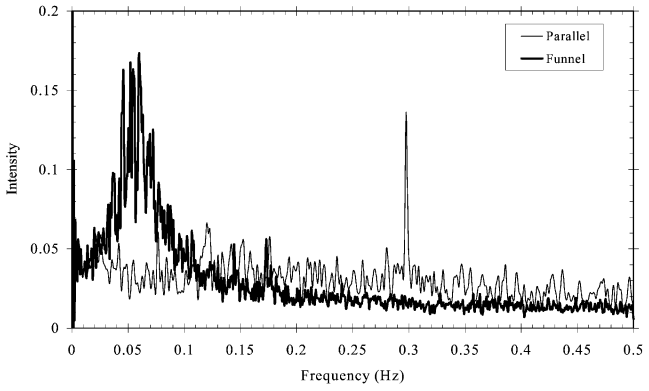

(*a*)

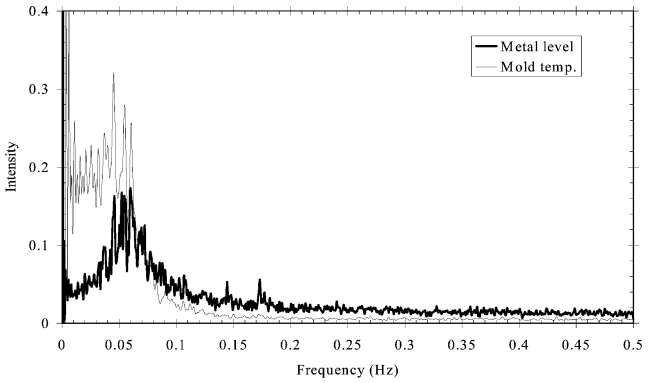

(*b*)

Fig. 23—Power spectra for the metal level and temperature response: (*a*) comparison of the metal level between the parallel and funnel molds and (*b*) comparison of metal level and temperature response in the funnel mold.

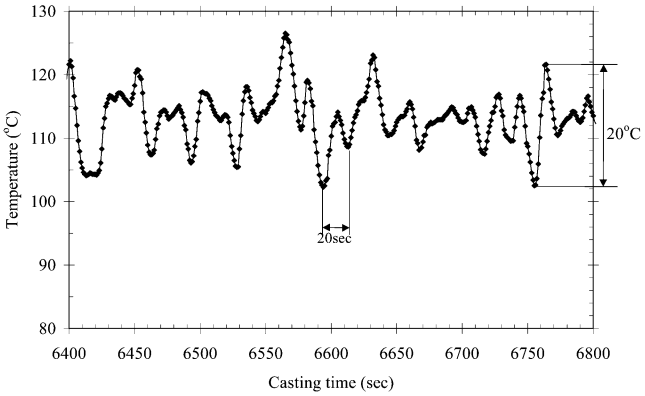

(*a*)

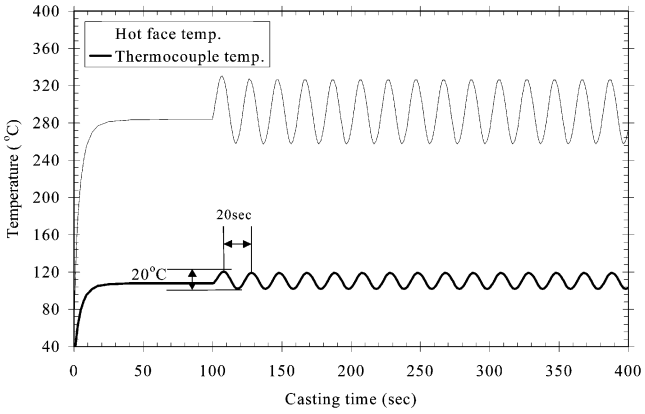

(*b*)

Fig. 24—Thermal pattern of the funnel mold at the meniscus: (*a*) measured temperature profile at the thermocouple position and (*b*) calculated hot face and thermocouple temperature.

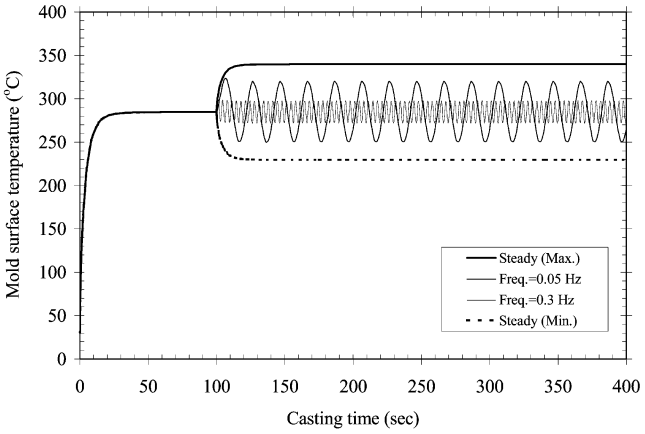

Fig. 25—Transient hot face temperature response for the various cases of thermal cycles.

from the 3-D analysis (3-D quarter model), described in Part I, were imposed as fixed-displacement boundary conditions on each tension bolt position in the 2-D quarter model. For example, Figure 9 shows the displacement boundary condition imposed on the 2-D quarter model at the position of 376 mm from the parallel mold centerline to realize the pretension force. Table II shows the maximum displacement at other bolts.

During heat up at the start of each continuous-casting sequence, there is some slight sliding between the mold and the backing plate (water box), which causes the tension bolts to move relative to the bolt holes. Since there are no threads for the tension bolt in the water jacket itself, the constraint condition due to the contact is governed by the clearance between the bolt and the bolt hole in the water jacket. As can be found from Table I, this clearance is 4 mm. This is safely larger than both the dimensional changes of the tension bolt diameter, which are less than 0.2 mm, and its horizontal movement, which is a maximum of 1.36 mm at the farthest bolt from the centerline. Thus, the contact surface between the mold plate and the water jacket is relatively free to slide in the width direction as friction was found in Part I to be negligible. Mathematically, this can be represented with interface elements to simply prevent penetration of the copper plate into the water box. This justifies the boundary conditions used on the 3-D quarter model in Part I.

Constraints in the horizontal plane were obtained at each thermal cycle from the results of the 3-D quarter model described in Part I. They were applied as fixed-displacement boundary conditions at the interface of the mold and water jacket of the 2-D quarter model at the bolt locations. Figure 10 shows the constraints imposed to restrain expansion in the thickness direction on the parallel mold during heat up at steady-state operation. Further details of the elastic-plastic-creep stress model, including the temperature-dependent yield-stress function for isotropic hardening and the equation for primary creep of Cu-Cr-Zr, are given in Part I.

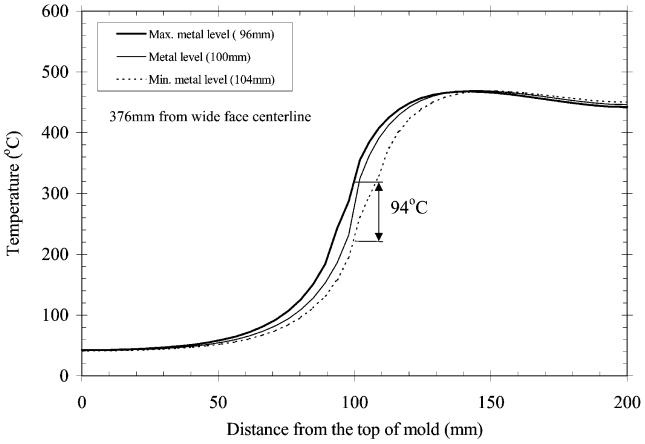

Fig. 26—Effect of the metal level on the hot face temperature predictions (3-D segment model).

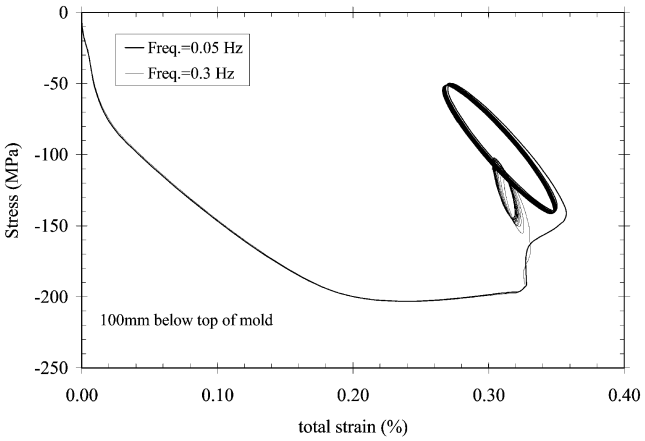

Fig. 27—Stress-strain hysteresis loop at the meniscus hot-face surface for the funnel mold with different frequencies of metal level fluctuation.

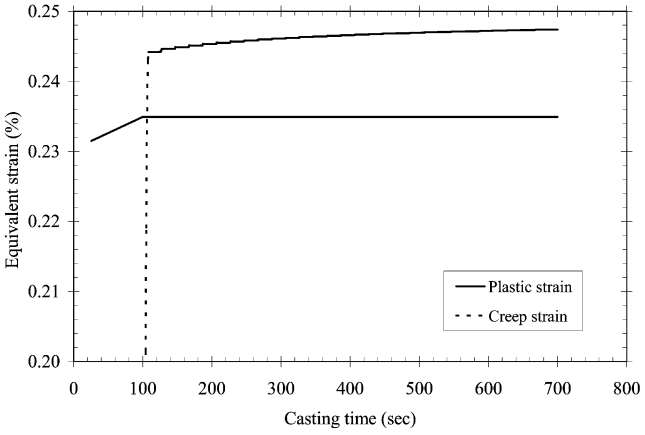

Fig. 28—Inelastic strain profiles with casting time.

Temperature profiles around the meniscus and crack region are studied using the 3-D segment model and the heat-flux data obtained in Part I. An attempt has been made to refine the heat-flux profile predictions around the meniscus region. There are many popular forms of empirical equations for the heat-flux profile as a function of distance in the mold.[10–14] Among them, the following three functions were selected for fitting the heat-flux profile:.

$$q_1\ (\mathrm{kW/m^2}) = 6107 - 821 \cdot t\ (\mathrm{s}) \qquad \text{Linear function [1]}$$

$$q_2\ (\mathrm{kW/m^2}) = 8420 - 2987\ \sqrt{t\ (\mathrm{s})}$$

Square root function [2]

$$q_3\ (\mathrm{kW/m^2}) = 6516 \cdot \exp\left[-0.2t\ (\mathrm{s})\right]$$

Exponential function [3]

Here, q is the heat flux (kW/m^2) down the mold length, and t is the residence time (seconds) of the strand below the meniscus.

Figure 11 compares the heat-flux profiles calculated along the centerline of the mold for these three equations. Note that all three profiles roughly satisfy the heat flux known at positions where thermocouple measurement were made (Part I). The meniscus heat flux is seen to vary from 8 to 6 MW/m^2, depending on the equation.

Next, this article presents results and discussion of several different studies using these models.

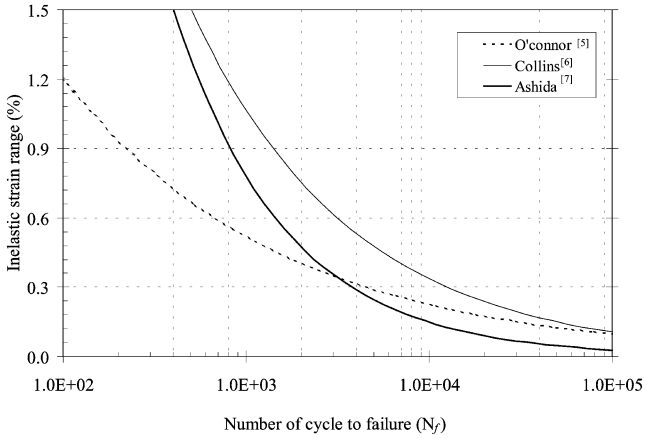

Fig. 29—Variation of cycle to failure for different fatigue models.

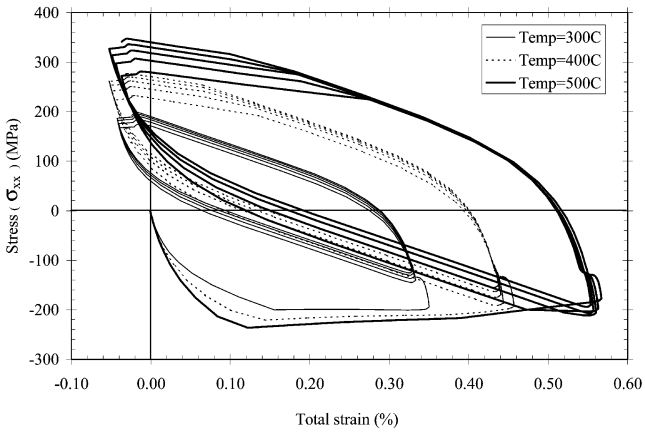

Fig. 30—Comparison of the stress-strain hysteresis loop with different hot face temperature for the funnel mold.

V. COMPARISON OF FUNNEL AND PARALLEL MOLD THERMAL-MECHANICAL BEHAVIOR

To isolate the effect of mold shape alone on temperature, stress, and crack occurrence, the same heat flux (4 MW/m^2)

Table III. Summary of Predicted Fatigue Life with Different Thermal Cycles

	Inelastic Strain (Pct)	Number of Thermal Cycles to Failure			Number of Sequence Cycles to Failure (1 sequence = 4 Hours)		
		O'Connor	Collins	Ashida	O'Connor	Collins	Ashida
SEN change*	0.45	1489	5591	2148	1489	5591	2148
Long period (f = 0.05Hz)	0.11	71,696	93,306	15,223	99	129	21
Short period (f = 0.3Hz)	0.33	1,965,211	1,034,242	81,152	454	339	19

*Assumed to be period of start/stop of casting transitions (one sequence).

Table IV. Summary of Predicted Fatigue Life with Different Hot Face Temperatures

Hot Face Temperature (°C)	Inelastic Strain (Pct)	Number of Sequence Cycles to Failure		
		O'Conner	Collins	Ashida
300	0.45	1489	5591	2148
350	0.52	1001	4148	1757
400	0.59	707	3254	1474
450	0.66	519	2601	1261
500	0.74	379	2070	1076
550	0.85	259	1569	887

was imposed on 2-D quarter models of the funnel and parallel molds. Figure 12 compares the temperature distributions calculated along the hot face of the two molds. As seen in this figure, the funnel mold shows a variation of temperature across the mold width despite the constant heat flux. In particular, the region around the funnel transition region, where the cracks occurred, is hotter by about 40 °C. This phenomenon is attributed to local variations in the slot geometry for the funnel mold. As shown in Figure 13, the distance between the hot face of the mold and the slot root (slot depth) is not uniform across the funnel mold width. In particular, the funnel transition region has a slightly greater effective thickness, with slot roots ranging from 0 to 3 mm further from the hot face than the others. This is because the slots are machined to equal depths in groups of 3 or 4 slots.

Typical stress and strain results from the 2-D quarter model are shown in Figures 14 and 15. Figure 14 compares the Von Mises stress profiles across the hot-face width of both molds. Figure 16 compares the inelastic strain (equivalent plastic strain plus equivalent creep strain)[9] distributions across the hot face, together with the region of crack occurrence. Where the hot-face temperature is higher in the funnel mold, the stress and strain results are also higher. Thus, both of these fracture criteria correctly indicate the location of cracks and suggest a relationship with the water slot array.

To gain insight into the crack formation process, Figure 16 plots the evolution of stress and strain over an entire casting campaign at a meniscus position on the mold surface, located where cracks are formed. When the mold temperature increases from room to operating temperature, the mold tries to expand towards the molten steel but is constrained in x by the cold copper and in y by the bolts on the water jacket, forcing most of the mold into compression. The highest compressive stress occurs on the hot face of the mold where the temperatures are highest. This compressive stress causes plastic yielding accompanied with time by creep strain, leading to residual inelastic compressive strain in the hot face. Upon cooling, this strain causes the mold to try to bend but is once again restrained from doing so by the bolts against the backing plate. This causes the former hot face to go into tension, which might initiate a crack. The tensile stress increases after each cycle, encouraging crack propagation. Figure 17 compares the stress-strain hysteresis loop after 50 sequences for both mold types. The maximum tensile stress after cooling down seems to be slightly higher in the funnel mold, where the cracks occur.

The magnitude of the differences in both stress and strain between the cracked and noncracked locations is very small, however. Thus, these results explain only the location where cracks initiate in the funnel mold. They do not completely explain the difference in susceptibility between the funnel and parallel mold shapes.

VI. FUNNEL MOLD ANALYSIS USING TEMPERATURE AND CRACK MEASUREMENTS

A. *Measured Temperature Profiles*

To investigate the relationship between temperature profile, stress, and cracks near the meniscus, mold temperatures were measured at the meniscus in a funnel mold. Figure 18 shows the temperature response at different positions across the hot face at the meniscus during steady-state casting. The temperature 376 mm from the mold center is higher than other locations by 50 °C. This was expected, based on the analysis presented in Section V, due to slot variation. However, the same maximum temperature at this location was observed in the parallel mold, as described in Part I, so other phenomena appear to be important also.

B. *Simulations of Horizontal Profiles*

Based on the measured temperatures, the 2-D quarter model was used to calculate temperature, stress, and strain distributions in the funnel mold. Figure 19 shows the temperature distribution across the hot face and thermocouple location, including the corresponding artificially low heat-flux profile, adjusted for the 2-D quarter model mesh. It can be seen that hot-face temperature variation is significantly more severe than at the thermocouple depth. The funnel transition region is more than 70 °C hotter than the center region of the funnel mold. O'Connor and Dantzig[5] suggested that the outer bend of the funnel region is hotter due to convergent heat flow. This work, however, suggests that the peak in this region is greater and wider than can be explained by this phenomenon alone. It is also greater than could be expected from the local variations of water slot depth alone.

Stress and plastic strain in the transverse plane follow the temperature profile and have peak values that coincide with the region of crack occurrence, as shown in Figures 20 and 21. These results provide even stronger evidence that the cracks initiate in the funnel transition area due to higher temperatures in this region.

C. *Simulations of Vertical Profiles*

To investigate why the cracks form at their particular distance vertically down the mold, the hot-face temperature profile near the meniscus was simulated with the 3-D segment model using the three different heat-flux equations. Figure 22 shows the effect of the different heat-flux profiles on hot-face temperature predictions. Regardless of the exact equation, the peak temperature was always found about 20 to 30 mm below the molten metal level, which corresponds almost exactly with the region of crack occurrence. Some cracks were observed to extend to above the meniscus, where the temperature is relatively low. This was hypothesized to be crack propagation from cyclic fatigue due to metal-level fluctuations.

VII. METAL-LEVEL FLUCTUATION STUDY

A. *Metal-Level and Meniscus Temperature Fluctuation Measurement*

Metal-level fluctuations are a potential source of cyclic thermal loading on the mold. They can occur in spite of an automatic control system due to turbulence in the mold related to transient variation in the mold flow pattern. To quantify the magnitude and frequency of these fluctuations on meniscus temperature fluctuations, both metal-level signals and meniscus thermocouple measurements were analyzed using Origin.[15] Fourier analysis was applied to determine the frequency distribution of the metal-level signals of both the parallel and funnel mold based on the plant data presented in Part I. Figure 23(a) shows the computed intensities, which represent the relative contribution of each frequency to the overall level-fluctuation signal. It is evident that the funnel mold has mainly low-frequency level fluctuations, averaging about 0.05 Hz, compared to the generally high-frequency fluctuations of 0.3 Hz in the parallel mold. This corresponds to fluctuation periods of 20 seconds (funnel mold) and 3.3 seconds (parallel mold). The reason may be due to the thicker funnel mold, which contains more fluid volume, and delays the side-to-side transient sloshing observed by Honeyands *et al.*[16]

Next, the meniscus temperature variations measured at 100 mm below the top of the funnel mold were analyzed. Figure 23(b) compares the power spectra from both metal level and temperature response of the funnel mold. The measured temperature has a peak value at around 0.05 Hz, which corresponds exactly with the frequency of the metal-level fluctuations. Each temperature peak is clearly caused by a metal-level fluctuation. This agrees with the findings of Lai *et al.*[17] that mold thermal response provides a good indication of the meniscus-level fluctuation.

B. *Fluctuating Temperature Simulation*

The transient 2-D quarter model was applied to simulate the effect of metal-level fluctuations on temperature, stress, and strain variation near the meniscus. First, a sinusoidal heat-flux equation was adopted so that the temperature field produced by the 2-D quarter model matches with the measured temperature. Specifically, the artificially low heat flux was varied between 2.15 and 3.39 kW/m^2.

Figure 24(b) shows the calculated temperature histories at both the hot face and thermocouple locations. The thermocouple location shows a temperature range of 100 °C to 120 °C (an amplitude of 20 °C), which closely matches the measured thermal response in Figure 24(a). The corresponding hot-face location temperature varies from 260 °C to 325 °C (an amplitude of 65 °C), as shown in Figure 24(b). Having calibrated the model, the fluctuation frequency was varied. In order to isolate the effect of level fluctuation alone on temperature, stress, and strain, all other conditions were kept constant and both simulations were performed on the funnel mold geometry. Figure 25 compares the transient mold temperature response at high frequency (0.3 Hz), low frequency (0.05 Hz), and steady state, respectively. As shown in this figure, increasing the fluctuation frequency lowers both the peak temperature and its amplitude. Specifically, while the 0.3 Hz frequency has a temperature fluctuation amplitude of 20 °C at the hot face, the 0.05 Hz frequency has an amplitude of 75 °C. The temperature fluctuation at the thermocouple depth is much smaller (0.7 °C for 0.3 Hz and 20 °C for 0.05 Hz). At frequencies of 0.016 Hz or less, the temperature and stress amplitude are virtually the same as at steady state. In this case, hot-face temperature fluctuation can also be confirmed with calculations using the 3-D segment model. Figure 26 shows the effect of metal level on the steady-state hot-face temperature prediction, based on ±4-mm level changes. This was achieved by shifting the standard linear heat-flux profile in Figure 10 vertically by ±4 mm for the boundary conditions of the 3-D segment model. As can be seen, the amplitude of hot-face temperature variations at the meniscus (100 mm below the mold top) was about 94 °C (range of 228 °C to 322 °C), which is similar to the 2-D quarter model predicted amplitude of 110 °C (range of 230 °C to 340 °C).

C. *Stress-Strain Fluctuation Simulations*

Based on the preceding temperature fields, stress and strain were calculated for the different metal-level fluctuation frequencies using the 2-D quarter model. Figure 27 shows the stress-strain hysteresis in the hot face of the funnel mold. The x inelastic strain (plastic + creep + thermal strain in the width direction) per thermal cycle is about 0.033 pct (0.3 Hz) and 0.11 pct (0.05 Hz), respectively. This result suggests that low-frequency metal-level fluctuations may damage the mold more than those at high frequency. It is noted that the alternating stress and mean stress from the fluctuation of molten steel are both entirely compressive. Relative to detrimental tensile mean stresses, it is well-known that compressive mean stresses are beneficial.[18] For example, compressive stresses increase the fatigue strength of alternating high-cycle fatigue by more than 50 pct.[19] Although the level fluctuations create variations that are wholly compressive, tensile forces are created at the end of each sequence, as shown in Figure 16. Low-cycle fatigue cracks are the result of accumulated inelastic-strain damage coupled with tensile forces. Thus, it might be possible that

the increasing compressive-inelastic strains due to level fluctuations could cause faster propagation of the fatigue cracks.

Figure 28 shows the trend of plastic and creep strain for the case of low frequency of metal-level fluctuation. From this figure, it can be found that almost all of the plastic strain occurs at the first thermal-load step. The creep strain increases monotonically with time. Although the increase per cycle is small (only about 0.0002 pct), the large number of cycles allows a significant amount of creep to accumulate (*e.g.*, up to 0.14 pct after one 4-hour casting sequence of 720 cycles at 0.05 Hz). During the fluctuation of the molten-steel level, the mold fatigue life appears to be governed by the creep due to the cyclic thermal loading.

VIII. FATIGUE CRACK PREDICTION

In continuous casting, the fatigue load is generated by thermal cycling from both fluctuations of the metal level and major casting transitions, such as submerged entry nozzle (SEN), tundish, and ladle changes, *etc.* The latter have very low frequency and high amplitude compared to the rapid shallow-level fluctuations.

A. *Failure Criteria*

There is a paucity of fatigue-life data available for continuous molds, in particular Cu-0.1 pct Cr-0.15 pct Zr composition. One relevant equation is that reported by O'Connor, who used fatigue data for a Cu-2 pct Cr alloy, which was tested at 538 °C at a strain rate of 2×10^{-3} s^{-1}[20] and corrected for the presence of creep, suggesting the following fatigue equation for number of cycles to failure, N_f:[5]

$$N_f = 1.66 \times 10^2 \times (\Delta\varepsilon_{in})^{-2.75} \quad [4]$$

where $\Delta\varepsilon_{in}$ is the inelastic strain range (percent) of stress-strain hysteresis.

Another equation was developed by Ashida and Takao,[7] who conducted thermal fatigue tests for Cu-0.8 pct Cr-0.2Zr. Fully-reversed cycling, out-of-phase thermal conditions were employed, ranging from tensile stress at room temperature to compressive stress at 350 °C with a frequency of 4.11×10^{-3} Hz.

$$N_f = 7.08 \times 10^2 \times (\Delta\varepsilon_{in})^{-1.39} \quad [5]$$

This material and loading conditions are quite similar to that in the mold plates of this study.

Collins and Taplin[6] also conducted isothermal low-cycle fatigue for Cu-0.5 pct Cr-0.1Zr-0.03Mg material in strain control at temperatures up to 400 °C and frequencies of 0.0017 to 0.17Hz, suggesting the following equation:

$$N_f = 1.43 \times 10^3 \times (\Delta\varepsilon_{in})^{-2} \quad [6]$$

These test frequencies roughly correspond to level fluctuation cycles in the present work. Collins states that for transgranular fracture, such as mold cracks found in the present study, the fatigue equation is independent of temperature and frequency.[6].

Fatigue life predictions are plotted logarithmically against the inelastic strain with the different criteria in Figure 29. In general, it is known that the fatigue life is influenced greatly by alloy composition, grain size,[6,7] temperature,[20,21] cycling frequency,[22] holding time,[23,24] loading pattern,[25,26,27] surface condition of the sample, environment,[28,29] test method,[30] and other factors. Therefore, the differences in fatigue life are not unexpected. Unfortunately, none include any wholly compressive cycles, so the life cycle cannot be exactly predicted for the present conditions. Nevertheless, a rough estimate of continuous-casting mold lifetime was determined by applying the results of these three criteria.

B. *Lifetime Prediction*

In order to predict fatigue life, inelastic strain was determined from the stress-strain hysteresis loops for three different cases of metal-level fluctuation (0.05 Hz and 0.3 Hz) and SEN change (single thermal cycle defined in Part I). Fatigue life predictions using all three equations for the three different types of thermal cycles are summarized in Table III. Considering that the mold cracks were observed in the funnel mold within 70 sequences, the predicted number of cycles to failure from SEN changes alone is much longer than the actual life. When applying Eq. [4] through [6] to metal-level fluctuations, the lifetime is much shorter. This strongly implies that the metal-level fluctuations influence mold life significantly. With the possible exception of Ashida's fatigue Eq. [5], the results in Table III also reveal that low-frequency metal-level fluctuations, such as found in the funnel mold, are more harmful to the mold service life than the high-frequency fluctuations found in the parallel mold, despite their fewer numbers. Very low frequencies (*i.e.*, <0.016 Hz) are expected to begin to decrease fatigue susceptibility again, as the temperature distribution approaches steady state and the number of cycles lowers. The preceding fatigue predictions apply only to the copper base metal. If a coating material, such as Cr, is applied to the hot face of the copper mold, the predicted cycles to failure are expected to be longer. Once the Cr-coating layer no longer protects it, however, these results suggest that mold life will be very short and will be controlled by metal-level fluctuations, which is consistent with metallurgical observations in this study.

Figure 30 shows the stress-strain hysteresis loop for the funnel mold with different hot-face temperatures during five sequences. Steady state was reached after just one sequence cycle, which is similar to O'Connor and Dantzig.[5] As can be seen in this figure, with the increase of hot-face temperature, the inelastic strain range (width of the loop) increases significantly. Table IV summarizes the fatigue life prediction according to the hot-face temperatures with different fatigue equations for the case of SEN transition. Increasing temperature is naturally expected to reduce lifetime, due to higher strain amplitude (as shown) and from lower fatigue cycles to failure (not available).

IX. MECHANISM OF MOLD CRACK FORMATION

The results of this study suggest that the mold cracks begin with the cracking or loss of the protective Cr coating at the hottest portion of the hot face found just below the meniscus in the transition region of the funnel mold. This is followed by attack of the exposed copper by zinc from the molten steel. The Zn forms a brass alloy, which is susceptible to intergranular creep failure. Once a short, shallow

crack initiates, it acts as a stress raiser for crack propagation by thermal fatigue. Propagation is greatly aggravated by metal-level fluctuations, particularly the more severe low-frequency fluctuations.

To avoid cracks, it is important to decrease the hot-face temperature, which will not only reduce coating failure and embrittlement by zinc pickup but will also lower the maximum stress and inelastic strain. The hot-face temperature can be reduced with smaller, effective copper thickness, higher thermal conductivity, or increased cooling water velocity. It appears to be important to avoid uneven slot depths that increase hot-face temperature, particularly in the transition region of the funnel, which is more susceptible to high temperature, stress, and inelastic strain. Metal-level fluctuations must be avoided, particularly those at the most detrimental low-frequency range (about 0.01 to 0.2 Hz). Finally, it is important to minimize residuals, such as zinc, in the molten steel.

X. CONCLUSIONS

The formation of short, longitudinal hot-face surface cracks in the meniscus region of a funnel mold for casting thin slabs is investigated using metallographic studies and mathematical models. The mechanism of crack formation is identified, and the stress and strain predictions are also linked to known fracture criteria to predict the fatigue lifetime.

1. Initiation of the cracks is associated with intergranular embrittlement caused by brass formed by zinc attack from the molten steel after the loss of the protective Cr coating at the hottest portion of the hot face just below the meniscus.
2. The SEM examination of the cracks reveals a transgranular fracture surface and striation structure beneath the intergranular surface portion of the crack, indicating fatigue propagation.
3. The cracks are formed just below the meniscus in the transition region of the funnel mold because this location has the highest temperature, stress, and inelastic strain.
4. The slot depth of the funnel mold varies in distance from the hot face, ranging from 25 to 28 mm from the hot face in the funnel transition area, which contributes to higher stress and strain fields relative to the parallel mold.
5. The funnel mold was found to have metal-level fluctuations with a low frequency (0.05 Hz) relative to the parallel mold, which had a high frequency (0.3 Hz).
6. The low-frequency metal-level fluctuations are predicted to cause higher cyclic stresses and lower fatigue life, thus helping to explain why cracks were found only in the funnel mold.
7. Cracks might be avoided by avoiding Zn residuals in the steel, lowering hot-face temperature, reducing level fluctuations, and preventing coating failure.

ACKNOWLEDGMENTS

The authors thank POSCO for permission to publish this article. The authors are indebted to many people in the Technical Research Lab., POSCO. In particular, we acknowledge the support of Dr. S.Y. Kim, who supplied plant trial measurement data, and Mr. W.W. Hur and Dr. C.H. Yim, for their cooperation and assistance. The technical support of Neil Walker in conducting the mold crack analysis is warmly appreciated. The authors are also grateful for helpful discussions with Dr. T.J. Yeo and Mr. J. Shaver. Support of BGT from the Continuous Casting Consortium at the University of Illinois and from the National Science Foundation (Grant No. DMI 98-00274) is also acknowledged. Funding for this project from POSCO is gratefully acknowledged.

REFERENCES

1. A. Grill, K. Sorimachi, and J.K. Brimacombe: *Metall. Trans. B*, 1976, vol. 7B, pp. 177-89.
2. Y.M. Won, T.J. Yeo, K.H. Oh, J.K. Park, J. Choi, and C.H. Yim: *Iron Steel Inst. Jpn. Int.*, 1998, vol. 38 (1), pp. 53-62.
3. H. Gravemann, J.I. Brown, and C.D. Tapley: *Continuous Casting of Steel, 2nd Process Technology Conf.*, Chicago, IL, Feb. 1981, vol. 2, pp. 23-25.
4. E.B. Hawbolt, F. Weinberg, and J.K. Brimacombe: *Continuous Casting*, AIME, Warrendale, PA, 1984, vol. 2, pp. 85-102.
5. T.G. O'Connor and J.A. Dantzig: *Metall. Trans. Mater. B*, vol. 25B, 1994, pp. 443-57.
6. A.L.W. Collins and D.M.R. Taplin: *Advance in Research on the Strength & Fracture of Material*, 1977, pp. 839-47.
7. S. Ahida and T. Takao: *Hitachi Zosen Tech. Rev.*, 1984, vol. 45 (2), pp. 70-76.
8. H.O. Fuchs and R.I. Stephens: *Metal Fatigue in Engineering*, John Willey & Sons Inc., New York, NY, 1980, pp. 30-31.
9. *ABAQUS, Post Manual*, Hibbitt, Karlsson & Sorensen, Providence, RI, 1996, pp. 4.1.1-4.1.7.
10. D.P. Evteev: *Stal in English*, 1969, vol. 20, pp. 708-11.
11. E.A. Upton, T.R. Satya Rao, P.H. Dauby, and R.C. Knechtges: *Iron Steelmaker*, 1988, vol. 15 (5), pp. 51-57.
12. R. Davies, N. Blake, and P. Campbell: *Proc. 4th Int. Conf. on Continuous Casting*, Brussels, Belgium, 1988, vol. 2, pp. 645-54.
13. J. Konishi: *Masters Thesis*, University of British Columbia, Vancouver, BC, Canada, 1996.
14. S. Hiraki, K. Nakajima, T. Murakami, and T. Kanazawa: *77th Steelmaking Conf. Proc.*, ISS-AIME, Warrendale, PA, 1994, vol. 77, pp. 397-403.
15. *Microcal Origin 6.0*, Microcal Software Inc.
16. T. Honeyands, J. Lucas, J. Chambers, and J. Herbertson: *Steelmaking Conf. Proc.*, Toronto, Apr. 1992, vol. 75, pp. 451-59.
17. W. Lai, M. Milone, and I.V. Samarasekera: *83rd Steelmaking Conf. Proc.*, ISS-AIME, Warrendale, PA, 2000, vol. 83, pp. 261-74.
18. M. Klesnil and P. Lukas: *Materials Science Monographs*, Elsevier, Amsterdam, 1980, vol. 7.
19. P. Lukas and L. Kunz: *Int. J. Fatigue*, 1989, vol. 11, p. 55.
20. NASA-CR-121259, N74-14190, Mar-Test Inc., Cincinnati, OH, 1973.
21. S.S. Manson: *Thermal Stress and Low-Cycle Fatigue*, McGraw-Hill, New York, NY, 1966.
22. G.J. Cocks and D.M.R. Taplin: *J. Aus. Inst. Met.*, 1975, vol. 29 (4), pp. 210-19.
23. R.A.T. Dawson: *Conf. Thermal and High Strain Fatigue*, Institute of Metals and Iron and Steel Institute London, 1967, pp. 416-17.
24. D.J. White: *Proc. Inst. Mech. Eng.*, 1969–70, pp. 223-40.
25. R. Eckert, C. Laird, and J. Bassani: *Mater. Sci. Eng.*, 1987, vol. 91, pp. 81-88.
26. A.J. Mcevily, Jr. and R.C. Boettner: *Acta Metall.*, 1963, vol. 11 (7), pp. 723-43.
27. J.C. Earthman and W.D. Nix: *Acta. Metall.*, 1987, vol. 35 (2), pp. 463-72.
28. L.F. Coffin: *J. Mater.*, 1971, vol. 6, pp. 388-402.
29. D. Tromans and R.H. Sun: *Mater. Sci. Eng.*, 1996, vol. A219 (1–2), pp. 55-65.
30. B. Tongma and C. Laird: *Mater. Sci. Eng.*, 1990, vol. 213 (2), pp. 159-67.

Summary of Comments on METB02C272

Page: 7

Sequence number: 1
Author: IPC
Date: 2/28/2002 11:41:57 AM -24'00'
Type: Note
Au: Vendor name and locatin?

Page: 10

Sequence number: 1
Author: IPC
Date: 2/28/2002 11:42:25 AM -24'00'
Type: Note
Au: Table III: Column head for column 1?

Page: 13

Sequence number: 1
Author: IPC
Date: 2/28/2002 11:43:49 AM -24'00'
Type: Note
Au: Reference 3: Publisher name and location? Year of publicatoin?

Sequence number: 2
Author: IPC
Date: 2/28/2002 11:44:05 AM -24'00'
Type: Note
Au: Reference 4: Location correct?

Sequence number: 3
Author: IPC
Date: 2/28/2002 11:46:29 AM -24'00'
Type: Note
Au: Reference 6: Is this a book? Publisher name and location?

Sequence number: 4
Author: IPC
Date: 2/28/2002 11:46:56 AM -24'00'
Type: Note
Au: Please verify the title? Is this an English translation?

Sequence number: 5
Author: IPC
Date: 2/28/2002 11:47:26 AM -24'00'
Type: Note
Au: Reference 12: Publisher name and location? Year of publication?

Sequence number: 6
Author: IPC
Date: 2/28/2002 11:47:55 AM -24'00'
Type: Note

Au: Reference 15: Location of publisher? Year?

Sequence number: 7
Author: IPC
Date: 2/28/2002 11:48:18 AM -24'00'
Type: Note

Au: Reference 16: Publisher name and location? Year of publicaton?

Online Proofing Guidance Page

FIRST STEP:

Install Adobe Acrobat Reader if you do not already have this or another Acrobat product installed on your computer. You can do this free of charge by connecting to the Adobe site and following the instructions at:

http://www.adobe.com/products/acrobat/readermain.html

SECOND STEP:

Please download and print your PDF file — we recommend that you save this file to disk, rather than opening it from within your Browser.

From a PC:

1. Right-click on the file/article link.
2. Select ''Save Target as''
3. Select a desired location on your computer to save the file to, and click on ''Save''
4. Open your PDf file directly with Acrobat Reader or another Acrobat product.
5. Print this file as you normally would with any typical application. Example: Go up to your toolbar, select ''File'', select ''Print''.

From a MAC:

1. Hold the mouse button down over the link.
   a. In Internet Explorer, select ''Download Link to Disk'' from the resulting pop-up menu
   b. In Netscape, select ''Save this Link as'' from the resulting pop-up menu
2. Select a desired location on your computer and click on ''Save''
3. Open your PDF file directly with Acrobat Reader or another Acrobat product.
4. Print this file as you normally would with any typical application. Example: Go up to your menu bar, select ''File'', select ''Print''.

THIRD STEP:

Please go through the file you have just printed and thoroughly and clearly mark any revisions you would like to see implemented in your paper. If you have had any changes in phone/fax or e-mail addresses since your paper was submitted, please send us this new information.

FOURTH STEP:

Your revised paper needs to be faxed or mailed to:

IPC Communication Services
Attn: Sheryl Dickenson
501 Colonial Drive
St. Joseph, MI 49085
Fax number: 1-616-983-4064

If you have questions regarding your paper in general, you may email or telephone:

IPC Communication Services
Attn: Sheryl Dickenson
Email: sdickens@ipcjci.com
Phone: 1-616-983-7412, ext. 529